Bidirectional Capacitive Wireless Power Transfer for Energy Balancing in Modular Robots

Akshay Sarin, Duncan Abbot, Shai Revzen, Al-Thaddeus Avestruz
Department of Electrical Engineering and Computer Science
University of Michigan
Ann Arbor, MI 48109
Email: akisarin@umich.edu

Abstract: A modular approach to the complex robotic systems is desireable due to advantages such as ease of development, reconfigurability, and re-usability. Powering these dynamic structures while maintaining ease of assembly and versatile form-factor is a challenge. One promising solution is to exchange energy between modules which each have a small battery. Performing this exchange of energy using mechanical connections is not only unreliable but also limits the reconfigurability of the modules. In this paper, we present a bidirectional capacitive wireless power transfer scheme for energy balancing between different robot modules. A modified CMCDE topology is also presented to make the power transfer resilient to the changes in the robot dimensions. The concept is verified by demonstrating 20 W of power transfer between two modules at 13.56 MHz achieving a dc-dc efficiency of 79 % that is resilient to the changes in the track length.

I. Introduction

Robots are being used in more diverse, dangerous and distant environments than ever before. To make these robots cheaper and more adaptable, creating modular robotic systems has become an increasingly popular goal [1] [2] . In applications such as space exploration and colonization, rescue missions, and emergency operations, easily re-configurable modular robots often out-perform traditional fixed structure robots [3] [4]. However, powering a dynamic structure such as a modular robot, while maintaining ease of assembly and form-factor versatility, is a challenge [5]. One solution is to equip each actuator module with local energy storage (a small battery) and charge the modules as needed. However, the rate of battery exhaustion of each module will be different based on the function of the module. Hence, this will limit the robot's operation time to the time it takes for the most power-hungry module to drain its local battery. A possible solution to overcome this problem is to have the modules share energy amongst themselves. This will allow a lesser-used module to transfer the unused energy to the power-hungry module. In this paper, we provide a contactless solution to enable energy exchange among the different modules.

The exchange of energy between modules can be performed with a galvanically-wired connection and conductive connectors. Each module can further be equipped with power converters to control the flow of energy. However, the use of any mechanical connectors limits the self-reconfigurability of the modules. These connectors are also unreliable and wear out over time causing unexpected electrical failures [6] [7]. The wear and tear also limit the operation in extreme conditions like corrosive (underwater) environments or high vibration surroundings. Wireless power transfer is, therefore, an attractive solution to eliminate the mechanical connectors in modular robots and enable energy exchange between these modules. Inductive wireless power transfer solutions have been proposed in the past for powering robots [5], [8]. However, using inductive power transfer for a modular structure would require pickup coils to be placed on the adjacent modules and the robot body. The requirements of the pick-up coil can be a hindrance to the flexibility of modular structures.

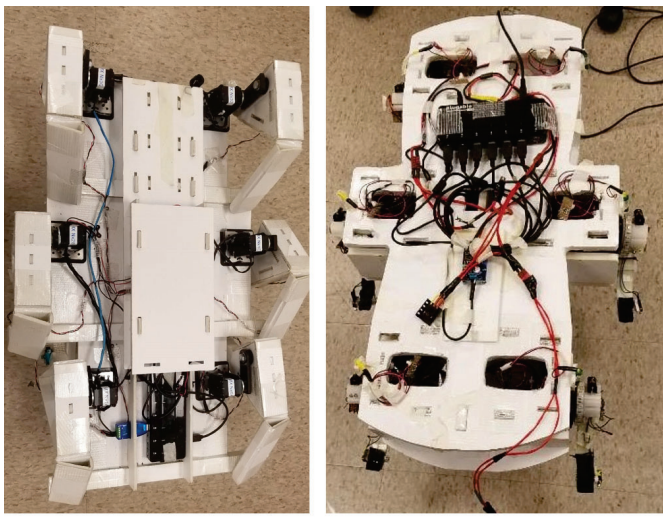


Fig. 1. a.) Big Ant modular robot. b.) Big Ant robot powered using galvanic wired connections.

An alternative to inductive wireless power transfer is to employ a capacitive wireless power transfer (C-WPT) scheme for energy balancing of wireless interchangeable robotic modules (WIRMs). C-WPT is an attractive choice for modular robots because the electric fields can be more easily confined [9]. In [10] the capacitive coupling between the modules was used as an electrostatic latch, utilizing the electrostatic force between the plates. We use the capacitive coupling between

978-1-7281-4829-8/20/$31.00 ©2020 IEEE

Authorized licensed use limited to: University of Michigan Library. Downloaded on November 14,2026 at 04:28:06 UTC from IEEE Xplore. Restrictions apply.

the robotic module and a conduction track on the body of the robot to enable power exchange between the modules for energy balancing. For small modular robots, made of non-conductive composite materials like fiberglass, using C-WPT is an attractive solution. The big ant robot shown in Fig. I is an example of such a modular robot. The big ant is equipped with identical modules in each of the six limbs. Depending on the terrain one limb may be used more than the other. Using C-WPT for energy exchange between different limbs can help prolong the operation time of the big ant.

Capacitive wireless power transfer has garnered a lot of attention in the past decade with applications that include electric vehicle charging [11], charging biomedical implants [12], charging of portable electronic devices [9], and powering robots [13]. In this paper, we present a capacitive wireless power solution to enable energy exchange among WIRMs. A modified current-mode class-DE (CMCDE) topology is presented that consists of a switched parallel resonant circuit driving a series resonance. The topology can be designed to be resilient to nominal changes in the robot dimensions by appropriately selecting the resonant components. Section II of the paper describes the basic principles for energy exchange among the modules. Section III describes the potential power converters for accomplishing energy exchange. Section IV presents the design and analysis of our modified CMCDE topology. Section V presents a design example and Section VI presents the our implementation. n

II. Basic Principle of Wireless Exchange between Modules

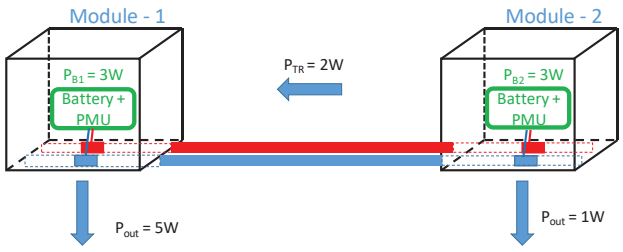


Fig. 2. Two identical robotic actuator modules with different power outputs based on functional requirements of the robot. To balance the power drawn from the battery of each module, module-2 transfers ~ 2 W of power to module-1. The two modules can exchange energy by capacitively coupling to the conduction track.

Modular reconfigurable robots can be valuable in unknown environments in what includes space exploration and rescue missions, among others. These robots can be made of small identical modules consisting of the actuators, a small battery (local storage), controller, and a power management unit (PMU). Based on the placement of these modules and the use of the robot, battery power at a particular module may be used up more quickly than the others. To enable the robot to function longer without charging, it is advantageous for the modules to share energy so that the aggregate battery use by the modules is balanced to the best effect. The average power

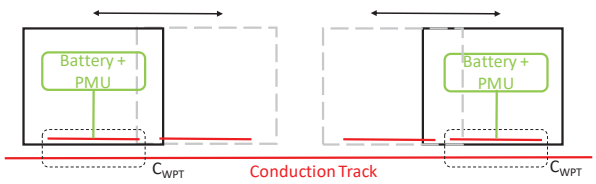


Fig. 3. Side-view for the WIRM actuators over the conduction track. The vertical distance between the track and the actuators determines the coupling capacitance. Thus, modules can slide horizontally over the track and maintain constant power transfer.

is balanced by wireless power transfer, while the peak power for any module is supplied by its battery.

Figure 2 shows the basic theory for energy balancing between two actuator modules. Module-1 and module-2 are two identical WIRMs used at different positions in a robot. The operation of the robot causes module-1 to be used more than module-2, hence the power drawn from the battery of module-1 is more than module-2. To balance the battery use of the two, module-2 can transfer power to module-1. To transfer, power between the modules, the wall of each module is capacitively coupled to a conduction track on the body of a robot as illustrated in Fig. II-A. The PMU of the transmitter module-2 converts the battery's dc power to RF power and delivers it capacitively to the conduction track. This RF power is picked up by the capacitive coupling between the receiver module-1 and conduction track and then converted to dc power for charging the battery.

A. Required Coupling Capacitance for Power Transfer

Each module is equipped with a copper plate at the boundary, which forms a capacitor with the track, and the non-conducting boundary acting as a dielectric for the capacitor. The size of each module limits the area of the copper plate, and the wall thickness determines the distance between the plates. For small robots, the capacitance is limited by the available area for given wall thickness. For example, for a given wall thickness of 0.25 mm, the capacitance per unit area is 3.5 pF/cm^2. For a plate area of 25 cm^2, the total plate capacitance is ~ 90 pF. However, the power transfer only depends on the vertical distance between the track and the module. From Fig. II-A, it can be observed that as long as the vertical distance between the track and modules remains the same, the magnitude of the power transfer will be almost constant, since the capacitance between the track and the module also remains the same. This WPT capacitance depends on the vertical distance and the area of coupling plates, so the modules can be sliding over the track and still maintain constant power transfer.

B. Track

The conduction track that is used to transfer the RF power can be made using copper foil or aluminum foil pasted to the body of the robot. The use of foil as a track thus preserves the

Authorized licensed use limited to: University of Michigan Library. Downloaded on November 14,2026 at 04:28:06 UTC from IEEE Xplore. Restrictions apply.

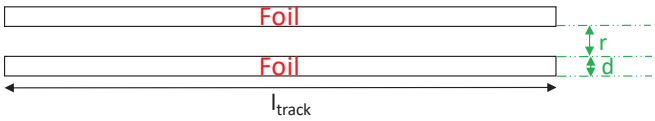


Fig. 4. The conduction track used on the body of the robot to enable energy exchange between the modules. The important parameters that determine the electrical properties (inductance, capacitance and resistance) are the length of the track (l_{track},), the distance between the parallel tracks, r and the thickness of the track, d.

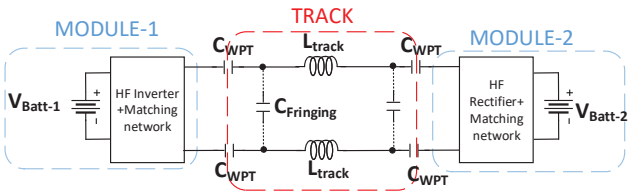


Fig. 5. Block diagram for capacitive wireless power transfer between module-1 and module-2. The track between the modules is modelled using lumped circuit elements since $l_{\text{track}} \ll \lambda$

flexibility of the structure. The track will behaves inductively as long as the length of track (l_{track}), is much less than the wavelength (λ) of the frequency selected for power transfer ($l_{\text{track}} \ll \lambda$). The inductance ($L_{\text{track}}$) of the track depends on the dimensions of the track,

$$L_{\text{track}} \approx \frac{\mu_0}{\pi} l_{\text{track}} \ln\left(4 + \frac{2r}{d}\right) \tag{1}$$

where r is the distance between the two tracks and d is the width of the track. Thus, for smaller lengths we can model the track as in Fig. 5, with a series inductance and a small fringing capacitance.

III. Power Converters for WPT between Modules

For transferring power through the coupling capacitance, the dc power from the battery has to be converted to a high-frequency ac power. Additionally, this power conversion must be carried out as efficiently as possible and the power converter operation must be tolerant to variation in the length of the track. It is also advantageous to have the same power converter being capable of receiving power as well, hence capable of acting as an active rectifier. Thus, the power-converter for accomplishing energy exchange between the WIRM modules should be both bi-directional [14] and resilient to the loading conditions. This can be accomplished by employing a high-frequency inverter with a matching network to compensate for the capacitance. A straight forward choice is to use a half-bridge or full-bridge inverter with a series resonance circuit [9]. The effective use of a half-bridge converter has previously been demonstrated for both sending and receiving power [15]. However, the use of the floating gate drives used for the half-bridge inverter limits the operating frequency hence the miniaturization of the robotic modules [16]. An alternative to using floating gate drives is to use a push-pull class-E converter [17]. Fig. 6 shows the schematic of a push-pull class-E converter employed for WPT between two modules.

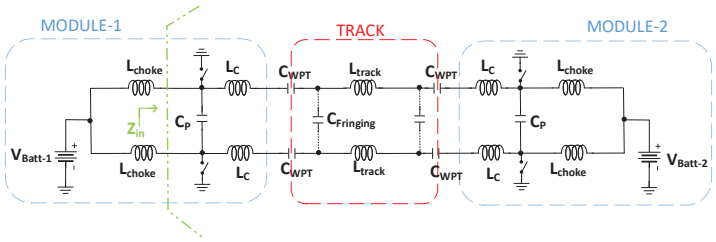


Fig. 6. Schematic for realizing bidirectional WPT between the actuator modules using push-pull class-E amplifier. The choke inductors carry the dc current. The track inductance, coupling capacitance and the compensating inductors all form a series resonant circuit.

The push-pull class-E consists of two ground-referenced switches and absorbs both the switch parasitic capacitance as well the track inductance in the resonant network. However, the push-pull class-E is not resilient to the changes in the track inductance. For achieving high-efficiency, the amplifier must employ zero-voltage switching (ZVS) to avoid the switching loss at higher frequencies. Hence for achieving ZVS, the input impedance, Z_{in} shown in Fig. 6 should be *inductive* [18]. The impedance, Z_{in} is given as :

$$Z_{in}(s) = \frac{1}{sC_P} || Z_s \tag{2}$$

where Z_s is given as

$$Z_s = s(L_c + L_{\text{track}}) + \frac{1}{s\frac{C_{WPT}}{4}} + \frac{1}{sC_P}. \tag{3}$$

Fig. 7 shows the variation of input impedance for a push-pull class-E amplifier. The input impedance is inductive (hence, achieves ZVS) only for a small range of frequencies. It can be observed from Fig. 7 that the input impedance of push-pull class-E amplifier becomes capacitive even for a small 10 % change in the series resonant inductor, hence looses ZVS. Thus, the push-pull class-E amplifier is not a suitable choice for modular, re-configurable robots, because the track inductance can vary depending on the size and the functionality of the robot.

To overcome the parameter sensitivity problem of the push-pull class-E amplifier, we propose a current-mode class-DE (CMCDE) amplifier shown in Fig. 8. The end-to-end circuit for WPT using CMCDE is very similar to the one using the push-pull class-E with an added parallel inductor, L_P. As will be discussed in the next section, the additional inductor provides another degree of freedom for making the design resilient to changes in the track inductance.

Authorized licensed use limited to: University of Michigan Library. Downloaded on November 14,2026 at 04:28:06 UTC from IEEE Xplore. Restrictions apply.

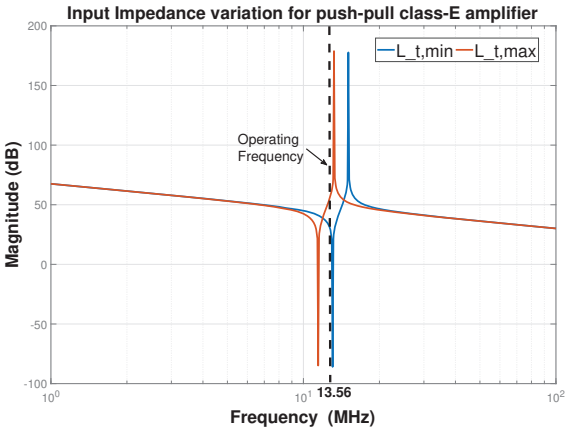


Fig. 7. Input impedance variation for a push-pull class-E amplifier. A 10 % variation of the series inductance , results in input impedance becoming capacitive at 13.56 MHz operating frequency, thus resulting in loss of ZVS.

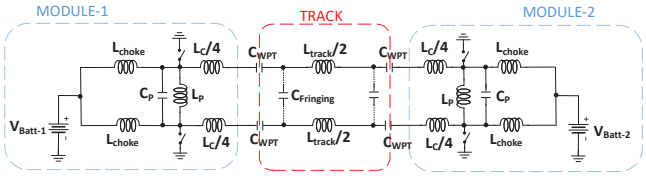


Fig. 8. Schematic for realizing bidirectional WPT between the actuator modules using the CMCDE amplifier. The CMCDE amplifier consists of CMCD tank at either end driving a series resonant circuit formed by the wall capacitance, the track, and the compensating inductor.

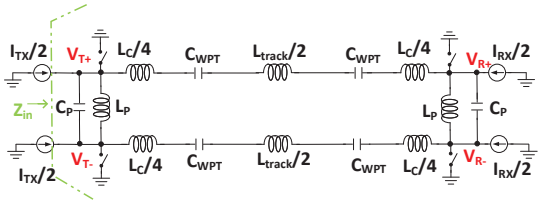
IV. CMCDE Analysis and Design

The CMCDE amplifier was first presented in [19] to achieve ZVS and zero voltage-derivative switching. This CMCDE amplifier consisted of a switched series-resonant circuit driving a parallel resonant tank. However, the CMCDE proposed in this paper has a switched parallel resonant tank driving a series resonance. The circuit is similar to that using push-pull class-E with an additional parallel inductance, L_P. In this section, we analysis and design technique for the proposed CMCDE amplifier for the C-WPT between modules is presented. For the purpose of design and analysis, the passive components are assumed to ideal and it is also assumed that the switching of the two modules undergoing energy exchange can be synchronized using a centralized controller.

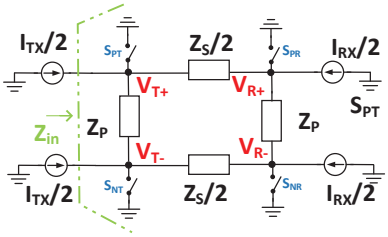
A. Analysis

The proposed CMCDE can be modeled as shown in Fig. 9 with the constant current source and a switched parallel resonant tank driving a series impedance. The input impedance for a CMCDE amplifier is

$$\begin{aligned} Z_{in} &= Z_P || (Z_P + Z_S) \\ &= \frac{Z_P(Z_P + Z_S)}{2Z_P + Z_S} \end{aligned} \tag{4}$$



(a) Equivalent circuit with the choke inductors replaced by constant current source.



(b) Equivalent circuit with abstracted impedances.

Fig. 9. Equivalent circuit representations for end-to-end WPT between two WIRMs using CMCDE amplifier

where the impedance Z_P is

$$Z_P = \frac{sL_P}{s^2 L_P C_P + 1} \tag{5}$$

and the impedance Z_S is

$$Z_S = s(L_C + L_{\text{track}}) + \frac{1}{s\frac{C_{WPT}}{4}}. \tag{6}$$

By appropriately choosing of the impedance, Z_P and Z_S we can make the input impedance Z_{in} be inductive for a wide range of track inductance, hence achieving ZVS.

The two switches of a module are operated in a complementary manner with a small overlap time between them, similar to a current mode class-D (CMCD) amplifier. Under the steady-state operating conditions, the dc voltage across the lossless choke inductors should be zero, hence

$$\overline{V_{T+}} = \overline{V_{T-}} = V_{dc_{TX}} \tag{7}$$

$$\overline{V_{R+}} = \overline{V_{R-}} = V_{dc_{RX}} \tag{8}$$

where $\overline{V}$ is average value of a variable over a switching period in steady-state, $V_{dc_{TX}}$ and $V_{dc_{RX}}$ are the battery voltages for transmitting and receiving modules respectively. Ideally, the modules are all identical and hence the battery voltages for the transmitting and receiving modules will be same, $V_{dc_{TX}} = V_{dc_{RX}}$. However, under different state of charge of the batteries the two dc voltages may also differ. For high-Q design, the drain voltages of each switch, i.e V_{T+}, V_{T-}, V_{R+}, and V_{R-} can be assumed to be approximately half-sinusoidal. Hence, the peak drain voltages are related to the dc voltage as

$$V_{T_{PK}} = V_{T+_{PK}} = V_{T-_{PK}} = \pi V_{dc_{TX}} \tag{9}$$

$$V_{R_{PK}} = V_{R+_{PK}} = V_{R-_{PK}} = \pi V_{dc_{RX}} \tag{10}$$

The phase-shift between the differential transmitting and

Authorized licensed use limited to: University of Michigan Library. Downloaded on November 14,2026 at 04:28:06 UTC from IEEE Xplore. Restrictions apply.

receiving voltages and the impedance Z_S calculated at the switching frequency determine the power transfer magnitude and direction. Let the transmitting end voltage be $V_{T_{PK}} \sin(\omega t)$, receiving end voltage be $V_{R_{PK}} \sin(\omega t + \theta_R)$ and the impedance be $Z_S \angle \theta_S$, then the power transferred can be approximated as:

$$P_{TR} = \frac{V_{T_{PK}} V_{R_{PK}}}{Z_S} \cos(\theta_S - \theta_R). \tag{11}$$

Thus, for a given phase-shift between two modules, the impedance of the series circuit determines the direction of power flow. The self-resonant frequency ω_s of the series impedance is $\omega_s = \frac{1}{(L_C + L_{\text{track}})\frac{C_{WPT}}{4}}$. If the switching frequency, ω is less than ω_s, the track impedance is capacitive, and for $\omega \geq \omega_s$, the track impedance is inductive.

The switching frequency, and the self-resonant frequency of the series impedance (the compensating inductors and the track) together determine the optimal phase difference between the transmitting and receiving module for maximum power transfer. Neglecting the losses in the series impedance, the optimal phase difference between the transmitting and receiving module is given as

$$\theta_R = \begin{cases} +90°, & \text{if } \omega \geq \omega_s \\ -90°, & \text{otherwise.} \end{cases}$$

B. Design

The goal of this section is to provide design guidelines for selecting the resonant components of the CMCDE amplifier, namely L_P, C_P, and L_C given the WPT coupling capacitance C_{WPT}, maximum track length, hence $L_{t_{MAX}}$, switch selection, and an operating frequency, f_{sw}. The coupling capacitance and the maximum track length are typically determined by the physical size of the modules. The switch and operating frequency selection can be performed by framing the optimization problem for maximizing the end-to-end efficiency of power transfer [20]. However, for the sake of simplicity, we will assume that the operating frequency and switch have been pre-determined.

The design steps for CMCDE amplifier design such that it is resilient to the changes in the track length are summarized as follows:

Step 1: Given the switch output capacitance (C_{OSS}), determine the parallel inductance L_P such that the parallel tank behaves inductively at the switching frequency. An external capacitance C_{ext} can be added for fine-tuning. To make the parallel tank inductive, the resonant frequency of the parallel tank, f_P should be slightly greater than the operating frequency, f_{sw}, i.e. $f_P > f_{sw}$.

Step 2: With the maximum track inductance, obtain the series inductance value such that the resonant frequency of the series impedance,Z_S is same as that of the parallel tank, i.e.

$$(L_C + L_{\text{track,Max}})C_{\text{WPT}} = L_P C_P \tag{12}$$

Step 3: Check if the input impedance, Z_{in} given in (4) is still inductive.

To understand the design process, consider the equivalent circuit Fig. 9b. For ideal operation, the series impedance, Z_S should be minimal and the parallel impedance should be as large as possible, i.e. $Z_S \to 0$ and $Z_p \to \infty$. Under these conditions, the track and WPT capacitance behave as a short circuit at the operating frequency. The series impedance,Z_S will act as short circuit ($Z_S \to 0$) at resonance and the parallel impedance, Z_P will act as an open circuit ($Z_P \to \infty$) at resonance. However, to achieve ZVS, both the tanks must be tuned at a frequency slightly above resonance [18]. The parallel impedance effectively acts inductance below the resonant frequency and the series tank effectively acts as a capacitance. Depending on the quality factors and the components selected the impedance, Z_2 shown in Fig. 10 will either behave inductively or capacitively. If Z_2 acts as an inductance, the overall inductance of the stage-1 will decrease and overall impedance Z_{in} will be inductive at the operating frequency. However, if the impedance, Z_2 is capacitive at the operating frequency, the series compensating inductor must be increased to maintain ZVS.

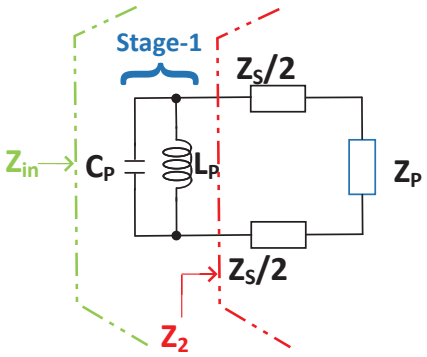


Fig. 10. The input impedance for end-to-end WPT among WIRMs using CMCDE amplifier.

V. Design Example

As an example design consider an application with the battery voltage of 20 V. A switching frequency of 13.56 MHz is selected and GaNFET, GS61004B (100 V, 15 mΩ) from GaN systems is chosen as the appropriate switch. A wall thickness of 0.2 mm with 5 cm × 5.5 cm copper plates yielding a WPT capacitance of ~ 125 pF. The track is also designed to have the same width as the copper foil with a spacing of 1 cm between the two parallel strips. The maximum length of the foil is assumed to be 40 cm, which gives a maximum track inductance of 250 nH. The minimum track length is assumed to be 20 cm, thus giving a minimum track inductance of 125 nH.

Step 1: The switch drain voltage for a dc voltage of ~15 V would be ~ 65 V. At this drain voltage the switch output capacitance is approximately 150 pF. For the parallel tank to be inductive $L_P \leq \frac{1}{w^2 C_P} = 760nH$.

Authorized licensed use limited to: University of Michigan Library. Downloaded on November 14,2026 at 04:28:06 UTC from IEEE Xplore. Restrictions apply.

!htb

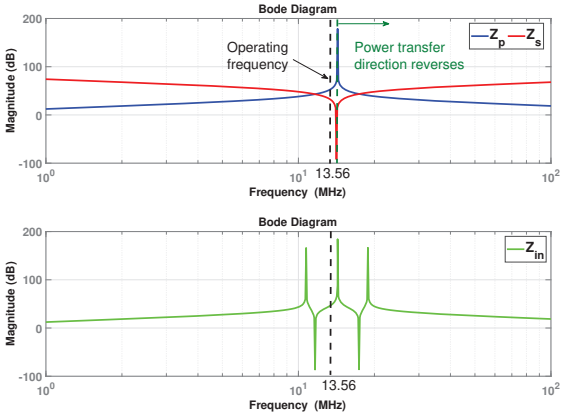


Fig. 11. Bode plot for impedance magnitudes of Z_P, Z_S and Z_{in}, with maximum track length. The resonant frequencies, f_P and f_S are chosen to be slightly higher than the operating frequency of 13.56 MHz. At this operating point the input impedance is indeed inductive.

!htb

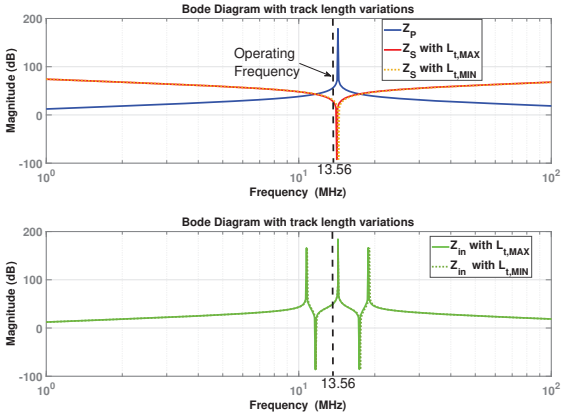


Fig. 12. Bode plot for impedance magnitude of Z_{in}, with variation in track length. The impedance, Z_{in} remains inductive under all variations of track length, thus the designed CMCDE amplifier will maintain ZVS under all track variations.

Choose $L_P = 530\,nH$ to account for switch non-linearity and other parasitic impedance. Simulation of the parallel circuit can be used to appropriately select parallel tank such that it behaves inductively at the operating frequency. The

Step 2: Obtain the series resonant inductor, L_{SR} that resonates with four series WPT capacitances of 125 pF at the operating frequency, $L_{SR} = \frac{1}{\omega \frac{C_{\text{WPT}}}{4}} = 4.4\,\mu H$.

Step 3: Choose a compensating inductor, L_C such that

$$L_C \leq L_{SR} - L_{t_{\text{MAX}}} = 4.15\,\mu H \qquad (13)$$

Using $L_C = 4\,\mu$H to account for model uncertainities.

Step 4: Check the input impedance Z_{in} for both $L_{t_{\text{MAX}}}$ and $L_{t_{\text{MIN}}}$ to ensure it is inductive, hence the converter will maintain ZVS under all possible track lengths.

Figure 11 shows the bode plot of magnitude of Z_P, Z_S and Z_{in}. For the chosen design, at the operating frequency, the series impedance is capacitive whereas the parallel impedance is indeed inductive. The magnitude of the parallel impedance at the operating frequency is greater than the series impedance, thus the effective input impedance a the operating frequency is inductive. If the operating frequency were to become greater than the series resonant frequency, f_S, for the same phase shift between the transmitter and the receiver module the power transfer direction would reverse, hence it is important that for all possible track lengths, f_S is greater than f. Since, the system is designed for the maximum track length with $f_S \geq f$, the reduction in track length (hence the increase in frequency f_S) will ensure that power transfer remains in the same direction. Additionally, from Fig. 12 it can be verified that the input impedance under the track variation indeed remains inductive, thus maintaining ZVS.

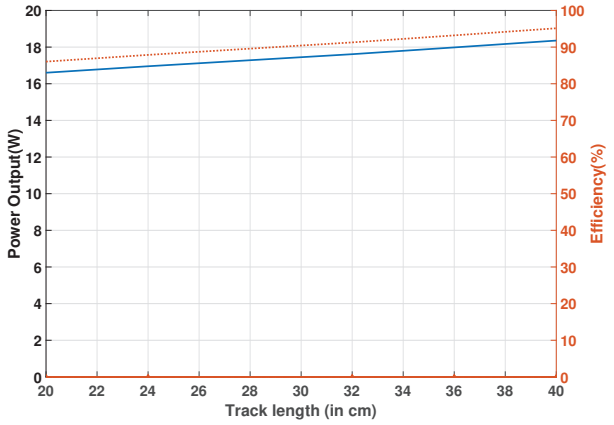


Fig. 13. Lt-spice simulation results for the chosen design using calculated values. The power-output and the efficiency are relatively constant across all track length, whose variation is captured in the inductance, L_{track}.

For the verification of the design, the system is modeled in LTspice with the obtained values. Fig. 13 shows the variation in power output and efficiency as a function of track length. It can be seen that the power output and efficiency levels are relatively constant. It should be pointed out though that LTspice models ignore the C_{OSS} loss [21], which can contribute to a significant portion of switch loss at 13.56 MHz.

VI. Hardware Design and Verification

For the implementation of WPT of WIRMs and the hardware verification of the design process outlined in the previous section, the track and the WPT capacitance are realized using the details described in table-I. Fig. 15 shows the image of the prototype hardware. The prototype hardware transfers

Authorized licensed use limited to: University of Michigan Library. Downloaded on November 14,2026 at 04:28:06 UTC from IEEE Xplore. Restrictions apply.

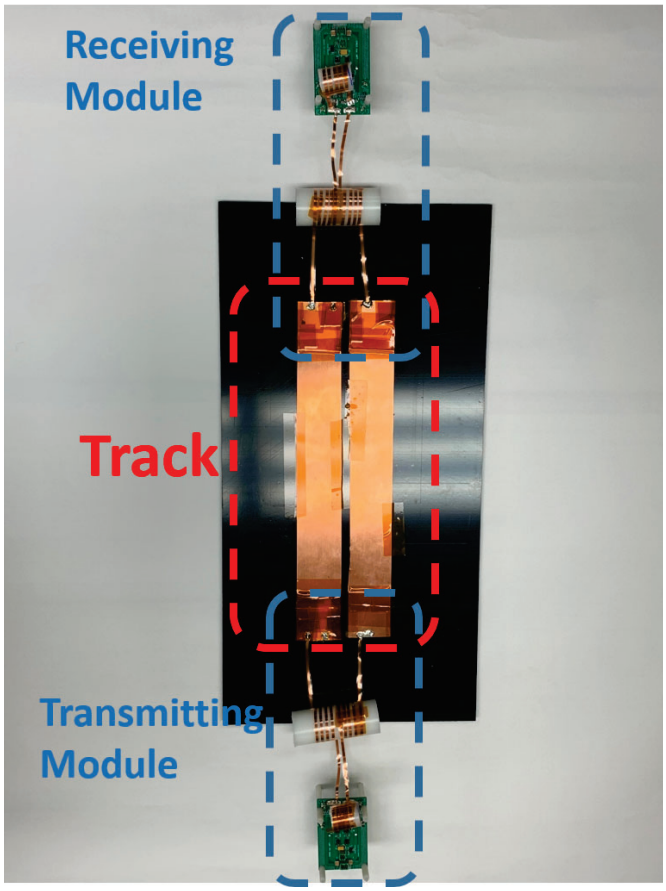


Fig. 14. Prototype hardware realization for bidirectional energy exchange. The coupling capacitor is realized using 28.5 cm^2 plates with 1/4 mm air gap giving a capacitance of ~ 125 pF. The conduction track is realized using 10 mil thick copper plates, 5 cm wide.

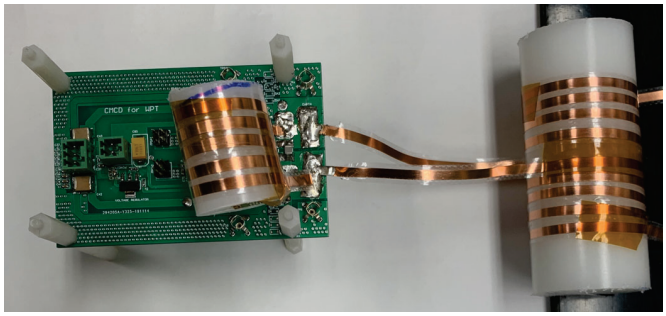


Fig. 15. The hardware prototype for CMCDE amplifier realized using GS61004B GaNFET and air core inductors.

TABLE I
COMPONENTS FOR HARDWARE DEMONSTRATION

Component	Value	Description
GaN FET	GS61004p from GaN systems	100 V, 15 mΩ, 120 pF
C_{WPT}	125 pF	Implemented between copper plates of dimensions 5 cm×5.5 cm
L_p	530 nH	Single layered solenoid made using 5-mil thick foil with 5 turns and 2.5 cm diameter
L_C	3.8 μH	Two center tapped air-core solenoids made using single-layer foil conductors with a diameter of 4 cm
C_p	33 pF	501S42E330JV3S from Johanson Technology
L_{choke}	56 μH	EPCOS B82111E Series
f_r	13.56 MHz	Resonant frequency
L_{track}	250 nH	Copper track made using 10 mil thick copper plates of maximum length 40 cm and width 5 cm

20.5 W of power with dc-dc efficiency of 78.8 % at a dc voltage of 20 V at each end. From Fig. 16 it can be seen that the GaNFETs indeed achieve ZVS on either side with the differential drain voltage at either end being approximately sinusoidal. The same hardware transfers 20.47 W of power at 78.32 % dc-dc efficiency for the minimum track length of 20 cm, thus confirming resilience to the changes in track-length.

Authorized licensed use limited to: University of Michigan Library. Downloaded on November 14,2026 at 04:28:06 UTC from IEEE Xplore. Restrictions apply.

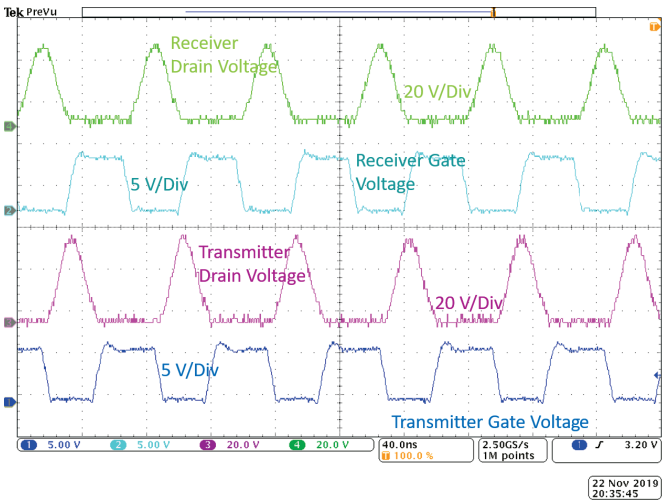


Fig. 16. Gate and Drain voltages for the transmitter and receiver switches. The switches on either-side indeed achieve ZVS thereby confirming the design.

VII. Conclusion

Exchanging electrical energy between dynamic structures in modular robots with small batteries is an attractive choice for powering these systems. In this paper, we presented a contactless solution for enabling bi-directional energy exchange between robotic modules. To transfer the energy between the modules, capacitive wireless power transfer is employed that uses a conduction track on the robot body for transferring power. We also presented a modified CMCDE topology for making the power transfer resilient to the changes in dimensions of the robot body. Prototype hardware is demonstrated that transfers 20.5 W of power with a dc-dc efficiency of 79 % for a track length of 40 cm. The prototype is resilient to the changes is track length and transfers 20.47 W of power at 78.32 % dc-dc efficiency for track length of 20 cm with the same hardware and same dc voltages at either end.

Acknowledgment

The authors would like to thank Xin Zan at University of Michigan for sharing perspectives on current-mode class-D amplifiers.

References

[1] A. C. Sanderson, "Modular robotics: Design and examples," in *Proceedings 1996 IEEE Conference on Emerging Technologies and Factory Automation. ETFA'96*, vol. 2. IEEE, 1996, pp. 460–466.

[2] I.-M. Chen and M. Yim, *Modular Robots*. Springer International Publishing, 2016.

[3] J. Seo, J. Paik, and M. Yim, "Modular reconfigurable robotics," *Annual Review of Control, Robotics, and Autonomous Systems*, vol. 2, no. 1, pp. 63–88, 2019.

[4] B. Salemi, M. Moll, and W.-M. Shen, "Superbot: A deployable, multi-functional, and modular self-reconfigurable robotic system," in *2006 IEEE/RSJ International Conference on Intelligent Robots and Systems*. IEEE, 2006, pp. 3636–3641.

[5] M. d. P. O. Cabrera, R. S. Trifonov, G. A. Castells, and K. Stoy, "Wireless communication and power transfer in modular robots," in *Proc. of IEEE/RSJ IROS: Workshop on Reconfigurable Modular Robotics: Challenges of Mechatronic and Bio-Chemo-Hybrid Systems*, 2011.

[6] N. Eckenstein and M. Yim, "Design, principles, and testing of a latching modular robot connector," in *2014 IEEE/RSJ International Conference on Intelligent Robots and Systems*. IEEE, 2014, pp. 2846–2851.

[7] M. Nilsson, "Essential properties of connectors for self-reconfiguring modular robots," 2001.

[8] H.-N. Kim, W.-Y. Chae, D.-S. Shin, H.-S. Kim, and H.-J. Kim, "The study on the wireless power transfer system for mobile robots," *World Academy of Science, Engineering and Technology, International Journal of Electrical, Computer, Energetic, Electronic and Communication Engineering*, vol. 4, no. 12, pp. 1744–1746, 2010.

[9] M. Kline, I. Izyumin, B. Boser, and S. Sanders, "Capacitive power transfer for contactless charging," in *2011 Twenty-Sixth Annual IEEE Applied Power Electronics Conference and Exposition (APEC)*. IEEE, 2011, pp. 1398–1404.

[10] M. E. Karagozler, J. D. Campbell, G. K. Fedder, S. C. Goldstein, M. P. Weller, and B. W. Yoon, "Electrostatic latching for inter-module adhesion, power transfer, and communication in modular robots," in *2007 IEEE/RSJ International Conference on Intelligent Robots and Systems*. IEEE, 2007, pp. 2779–2786.

[11] J. Dai and D. C. Ludois, "Capacitive power transfer through a conformal bumper for electric vehicle charging," *IEEE Journal of Emerging and Selected Topics in Power Electronics*, vol. 4, no. 3, pp. 1015–1025, 2015.

[12] K. Agarwal, R. Jegadeesan, Y.-X. Guo, and N. V. Thakor, "Wireless power transfer strategies for implantable bioelectronics," *IEEE reviews in biomedical engineering*, vol. 10, pp. 136–161, 2017.

[13] A. P. Hu, C. Liu, and H. L. Li, "A novel contactless battery charging system for soccer playing robot," in *2008 15th International Conference on Mechatronics and Machine Vision in Practice*. IEEE, 2008, pp. 646–650.

[14] X. Zan and A.-T. Avestruz, "27.12 mhz bi-directional wireless power transfer using current-mode class d converters with phase-shift power modulation," in *2018 IEEE PELS Workshop on Emerging Technologies: Wireless Power Transfer (Wow)*. IEEE, 2018, pp. 1–6.

[15] S. Sinha, A. Kumar, and K. K. Afridi, "Active variable reactance rectifier—a new approach to compensating for coupling variations in wireless power transfer systems," in *2017 IEEE 18th Workshop on Control and Modeling for Power Electronics (COMPEL)*. IEEE, 2017, pp. 1–8.

[16] D. J. Perreault, J. Hu, J. M. Rivas, Y. Han, O. Leitermann, R. C. Pilawa-Podgurski, A. Sagneri, and C. R. Sullivan, "Opportunities and challenges in very high frequency power conversion," in *2009 Twenty-Fourth Annual IEEE Applied Power Electronics Conference and Exposition*. IEEE, 2009, pp. 1–14.

[17] F.-Y. Chen, J.-F. Chen, and R.-L. Lin, "Low-harmonic push–pull class-e power amplifier with a pair of lc resonant networks," *IEEE Transactions on Circuits and Systems I: Regular Papers*, vol. 54, no. 3, pp. 579–589, 2007.

[18] R. W. Erickson and D. Maksimovic, *Fundamentals of power electronics*. Springer Science & Business Media, 2007.

[19] M. Matsuo, T. Suetsugu, S. Mori, and I. Sasase, "Class de current-source parallel resonant inverter," *IEEE Transactions on Industrial Electronics*, vol. 46, no. 2, pp. 242–248, 1999.

[20] J. R. Warren, K. A. Rosowski, and D. J. Perreault, "Transistor selection and design of a vhf dc-dc power converter," *IEEE Transactions on Power Electronics*, vol. 23, no. 1, pp. 27–37, 2008.

[21] G. Zulauf, S. Park, W. Liang, K. N. Surakitbovorn, and J. Rivas-Davila, "C oss losses in 600 v gan power semiconductors in soft-switched, high-and very-high-frequency power converters," *IEEE Transactions on Power Electronics*, vol. 33, no. 12, pp. 10 748–10 763, 2018.

Authorized licensed use limited to: University of Michigan Library. Downloaded on November 14,2026 at 04:28:06 UTC from IEEE Xplore. Restrictions apply.